PFM

JKU | Department of Particulate Flow Modelling

Annual Report | **2022**

EDITORIAL

Dear Readers,

"In between data and equations with physics governing everything"
This statement could serve as overall bracket of our current research activities.

Video coverage of experiments or just classical CFD simulations produce (a hell of) data, which can be seen as a natural playground for emerging data-based methods. Recurrence CFD efficiently exploits pre-calculated flow data while still considering physical conservation laws. We ride on data but obey physics! In the upcoming years, we will further explore rCFD's real-time capacities, aiming for the realization of digital rCFD twins of industrial processes.

However, we can still discover novel physical phenomena by just applying the fundamental flow equations. For instance, Mahdi Saeedipour disclosed the physics of the back-attack phenomenon during massive gas injection by thoroughly resolving the interaction between a super-sonic jet and the evolving gas-liquid interfaces. In the same project, Stefan Puttinger analyzed corresponding experimental videos by data-based methods.

These examples illustrate our strategy to use equations and data to explore physics!

With these introducing words, I wish you a pleasant reading!

All the best,

Stefan Pirker | stefan.pirker@jku.at

EDITORIAL

Dear Readers,

Time goes by and the Christian Doppler Laboratory for "Multi-scale modeling of multiphase flows" looks back to a successful research and cooperation with industry.

The last seven years were dedicated to application oriented fundamental research spanning from emulsions in stirred tank reactors, iron ore reduction in blast furnaces to polymerization in industrial scale fluidized bed reactors in steel and polymer industry.

At the beginning of the CD-Laboratory, we could not imagine what would be possible. But today, seven years later we are looking back to, for example, real time simulations of industrial scale polymerization gas-phase reactors or the detailed analysis of the iron ore reduction in industrial scale fluidized beds. We were exploring new technologies, such as the HYFOR process (hydrogen for ore reduction), and contributed to cutting edge research by investigating the nature of turbulence in multiphase flows.

This all would not have been possible without the trust and patience as well as the continuing support of the industrial partners. Here, I am looking forward to new challenges and research questions within the following research projects.

Finally, I have to especially thank all my coworkers including my motivated and hard working PhD students and Post Docs.

Sincerely,

Simon Schneiderbauer | simon.schneiderbauer@jku.at

CONTENTS

EDITORIAL | MICRO

Dear Readers,

In the past year, our research activities on micro-scale and resolved simulations have been further extended by a new life-science project funded by Linz Institute of Technology (LIT). **Carmine Porcaro** has joined us to carry out his PhD on multiscale modelling of blood flow where he aims at developing an engineering tool for the design and optimization of bio-microfluidic devices for plasma separation and passive diagnostic tests (Figure 1).

Within her PhD research, **Xiaomeng Zhang** has also made significant progress and could propose a physics-based criterion for the separation of micron-sized particles at the steel-slag interface (Figure 2). Such understanding at microscopic level could provide models for large-scale metallurgical systems for instance tundish simulations.

Furthermore, our research focus on the physics of turbulence in multiphase flows has further evolved, and we elaborated on how turbulence in multiphase flows can be described by the concept of vorticity transport equations. Also, we extended our portfolio of interfacial flow simulation toward the compressible regimes with applications in the steel industry.

Let's have a tour together to our research activities!

Mahdi Saeedipour | mahdi.saeedipour@jku.at
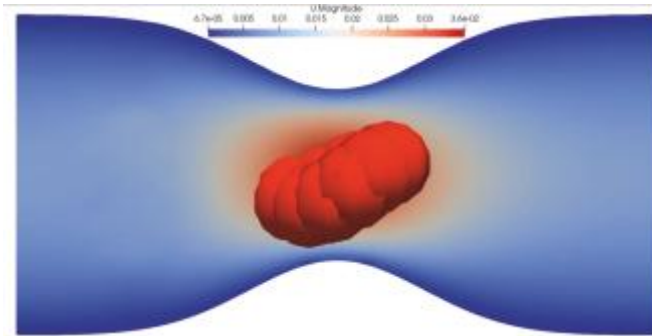
Fig.1: Deformation of a red blood cell across a converging-diverging microchannel pictured by reduced-order model in the context of resolved CFD-DEM. Such cell-level simulations are helpful in measuring the hemolytic damage in different microfluidic devices.
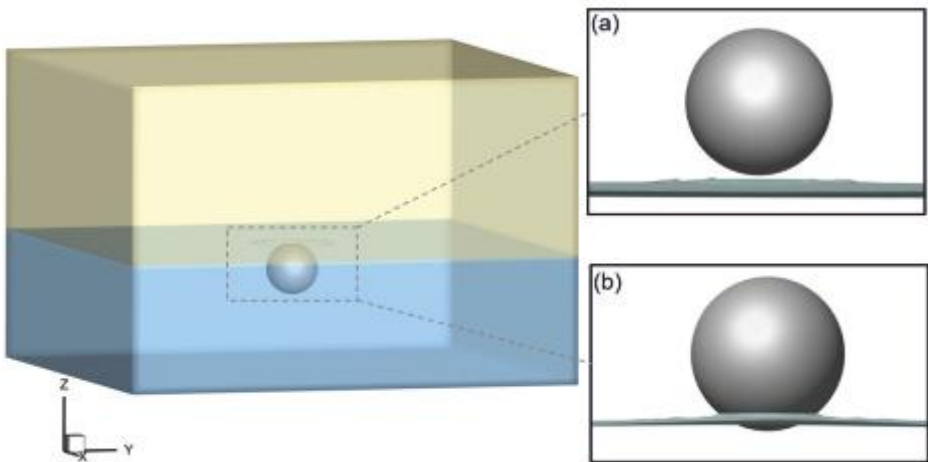
Fig.2: VOF-overset grid simulation of particle separation process at the fluid-fluid interface with the contact angle of (a) 20°, and (b) 40°. The snapshot on the left side provides a full view of the initial state in which the particle contacts the flat liquid-liquid interface.

MICRO | CFD-DEM SIMULATION OF BLOOD FLOW IN BIO-MICROFLUIDIC APPLICATIONS

Numerical simulation of blood flow is a challenging task in the biomedical research field. Analysis of bio-microfluidic devices requires cell-level resolution to correctly understand the underlying physics. In particular, small dimensions of these tools could cause strong deformation in the red blood cells (RBCs), leading to a phenomenon called hemolysis, namely hemoglobin leakage from RBCs. This may negatively affect safety and efficiency of clinical tests. Nevertheless, accurate membrane representation of RBCs requires a high amount of computational resources, which is not usually affordable for engineering applications. Thus, we employ a reduced-order RBC model for blood flow, based on an Immersed Boundary resolved CFD-DEM method. Each RBC is represented by a clump of overlapping rigid spheres connected by a fictional numerical bond, whose properties are tuned to reproduce the ones of RBCs viscoelastic membrane.

This year we first focused on further validation of the model in complex flow fields. Figure 1 presents the setup and the temporal evolution of one of these validation cases. The RBC is placed off-center into a stenosed channel, and replicates the deformation and orientation dynamics of previous numerical simulation studies which used more accurate and computationally expensive models. Then, we used a hemolysis model based on RBCs' deformation to understand the influence of several factors on hemolytic damage in microfluidic channels, such as shape, viscosity of the carrier fluid, and hematocrit. Results are presented in the form of a statistical analysis on RBCs population, then relevant biophysical quantities could be extracted from the numerical simulations, as the hemolysis index distribution (see Figure 2).

In future, we will focus on unresolved CFD-DEM simulation of deformable particles. This could allow the extension of blood flow simulation to real-scale biomedical devices with cell-level information.
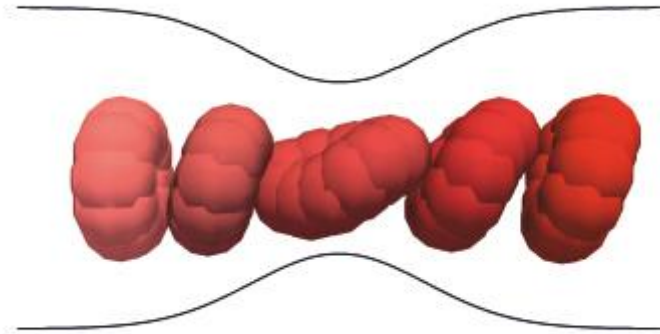
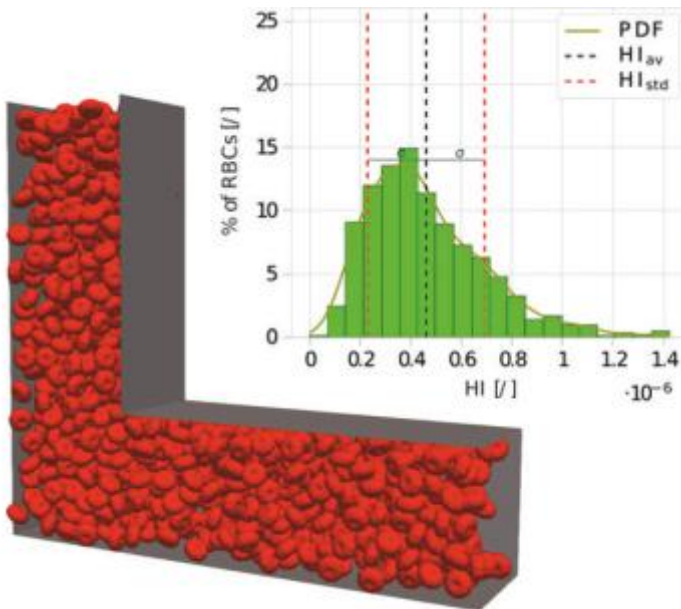**Fig.1:** Temporal evolution of an RBC passing into a stenosed channel.

Fig.2: Numerical simulation of 40% haematocrit blood flow in a microfluidic channel with hemolysis index distribution of RBCs at the exit.

Carmine Porcaro | carmine.porcaro@jku.at

MICRO | INCLUSION REMOVAL AT STEEL-SLAG INTERFACE: TOWARD A CRITICAL CONDITION FOR SEPARATION

Interactions between a fluid-fluid interface and a small impacting particle have a strong connection with the meniscus around the particle. The interaction sometimes renders a quasi-static state (such as in water-air systems) with the meniscus governed by the Young-Laplace equation. Given the particularity of the steel-slag system, that is high interfacial tension and fluid viscosities, it is featured by a prominent interfacial phenomenon upon the impact of the micron-sized inclusion particle, and meanwhile, the particle dynamics is difficult to be analytically studied. Currently, the separation of inclusion at the steel-slag interface has often been overlooked, even though it is an essential stage of the inclusion removal process.

Previously, particle motion at the steel-slag interface and the surrounding meniscus were successfully depicted by the dynamic overset grid-based multiphase CFD simulations (Figure 1). Then, a parameter study within the three-phase system is conducted to examine the most influential factors governing particle behavior (see Figure 2). The results indicate the dominant effect of the system's wetting condition and the slag viscosity on the maximum displacement of particle $(Z/R)_{max}$, which reflects the particle separation tendency. From an energy perspective, a better wetting condition generates more energy sources, and the interfacial energy is efficiently transformed into the particle's kinetic energy within a less-viscous environment, thus leading to better separation. Thus, we further develop a critical diagram (see Figure 3) that connects the particle dynamics (or particle surface energy, $\zeta =_l u_{max}^2 D_l$,) with the surface tension and viscous effects of fluids (reflected in a modified Reynolds number, $Re_\gamma = \rho_s \gamma_{MS} \gamma D_l / \mu_s^2$). Particle behavior in all simulation cases is clearly distinguished in terms of the two quantities.

The study on small-scale interfacial separation shows the possibility of being incorporated by large-scale simulations to improve the existing studies on inclusion removal in metallurgical vessels. The follow-up work will focus on implementing the removal boundary condition in the context of tundish flow simulation.
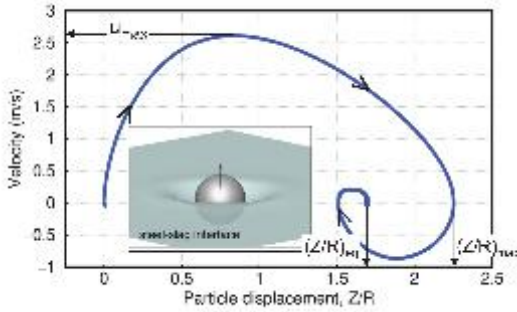
Fig.1: Particle's velocity-displacement curve with characteristic quantities highlighted (i.e., maximum position $(Z/R)_{max}$). Inserted figure shows the instantaneous meniscus around the moving particle.

Fig.2: Parameter study. Sensitivity of $(Z/R)_{max}$ to variations in three-phase contact angle θ, slag viscosity μ_s, interfacial tension γ_{MS}, particle size D_l and density ρ_l.

Fig.3: Particle behavior (separation or entrapment) in all simulations is distinguished based on the value of ζ and Reγ.

Xiaomeng Zhang | xiaomeng.zhang@jku.at

MICRO | INVESTIGATION OF MASSIVE GAS INJECTION INTO LIQUID

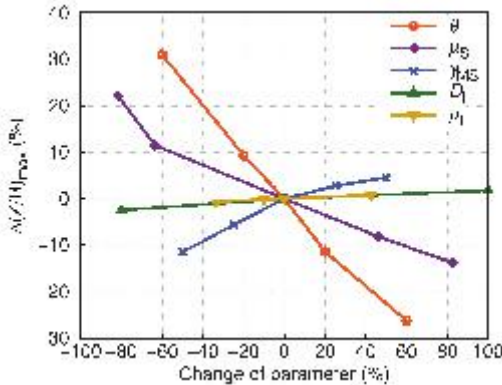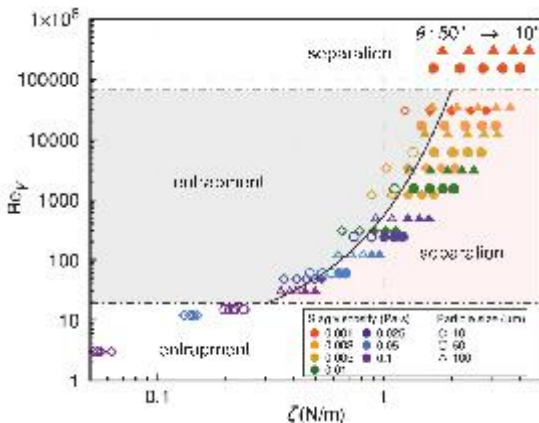Submerged gas injection into liquid is an effective way to intensify mixing and affect the chemical processes. Particularly in metallurgical processes, e.g. argon-oxygen decarburization (AOD) converter, high-speed injection of gas into molten metal leads to the reduction of dissolved carbon. Nevertheless, massive gas bellowing would entail several mechanical issues such as oscillations and refractory wears due to a phenomenon called "back-attack".

Massive gas injection in such extreme conditions usually involves various sources of complexity such as gas compressibility, interactions of turbulence with the liquid-gas interface, and shock dynamics. The high temperature in real metallurgical plants not only adds to the complexity but also makes any experimental characterization almost impossible. This challenges the numerical simulation and its potential experimental validation.

As a practical analogous system, we simulated the transonic and supersonic air injection into the water pool using the compressible VOF method. On the one hand, the presence of supersonic jets and shock formation demands a high temporal resolution for the simulations. On the other hand, the fragmentation of gas threads and bubble formation induces adds to the computational costs. Therefore, our preliminary study is focused on the near-injection region. We employed a k-equation large eddy simulation on rotational axisymmetric and symmetric domains. Various injection flow rates, according to the experiments, are tested as the initial conditions.

The simulation results demonstrate the supersonic regime inside the gas while penetrating the liquid. Figure 1 shows the formation of shock diamonds for the highest simulated gas flow rate. Besides, the liquid-gas interfacial structures are subject to instability and fragmentation due to the interactions with the shock wave propagation. The stronger the shocks are, the higher the instabilities would be, which eventually stimulates further fragmentation. The 3D simulations unveil this trend by the higher total interfacial area as shown in Figure 2. The preliminary results also disclose that the back-attack phenomenon may be explained by the shock reflection.

The validating experiments for such simulations are also designed (for further details see the experiments section on page 48). Further characterization of the flow and validations are planned for the next steps.
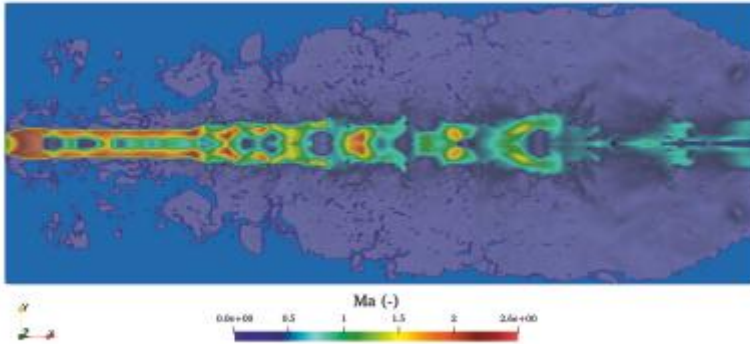
Fig.1: Instantaneous snapshots of the supersonic air injection into the water with Mach number contours and volume fraction iso-surfaces for injection pressure of 7.5 bar.
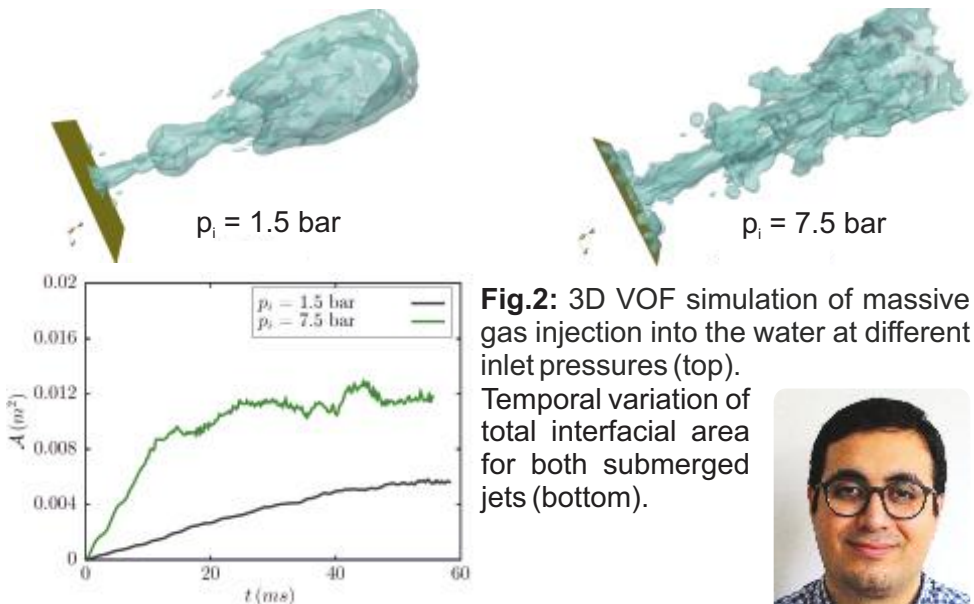

p_i = 1.5 bar

p_i = 7.5 bar

Fig.2: 3D VOF simulation of massive gas injection into the water at different inlet pressures (top).

Temporal variation of total interfacial area for both submerged jets (bottom).

Mahdi Saeedipour | mahdi.saeedipour@jku.at

MICRO | HOW DOES THE VORTICITY TRANSPORT EQUATION DESCRIBE MULTIPHASE TURBULENT PHENOMENA?

Understanding the evolution of turbulence in multiphase flows, compared to the single-phase ones, remains limited due to the complex inter-phase interactions across the scales. Due to the different origins of multiphase systems and their broad range of applications, one overarching question is raised: what do multiphase turbulent flows have in common?

We attempt to answer such fundamental questions and further deepen our understanding of multiphase turbulence by exploiting the classical concept of vorticity and its role in the evolution of the turbulent energy cascade. We start with the vorticity transport equations for two different multiphase flow formulations, which are one-fluid and two-fluid models. The former is used to describe the liquid-liquid interfacial flows, while the latter is commonly used to describe the gas-solid turbulence.

By extending the classical decaying homogeneous isotropic turbulence (HIT) problem to multiphase flow context, we perform fully-resolved simulations of the HIT problem in the presence of (i) a thin interface layer called interfacial-HIT and (ii) homogeneously distributed particles called particulate-HIT   (see Figure 1). Based on these highly-resolved simulations, we evaluated the spectral contribution of each production/destruction mechanism in the vorticity transport equation to the distribution of vortical energy. We base our discussion on the impact of the inter-phase interaction mechanisms, which are the surface tension for interfacial turbulence and drag force for particulate turbulence, and how their contribution to the vorticity transport impacts the evolution of the energy cascade.

Accordingly, our analysis provides an explanation for the differences between single-phase and multiphase turbulence cascades as shown in Figure 2, and proposes a valid approach for establishing a universal description of multiphase turbulence. These findings are essential to shape the next generation of subgrid models for large eddy simulations and multiscale modelling of large and complex systems.
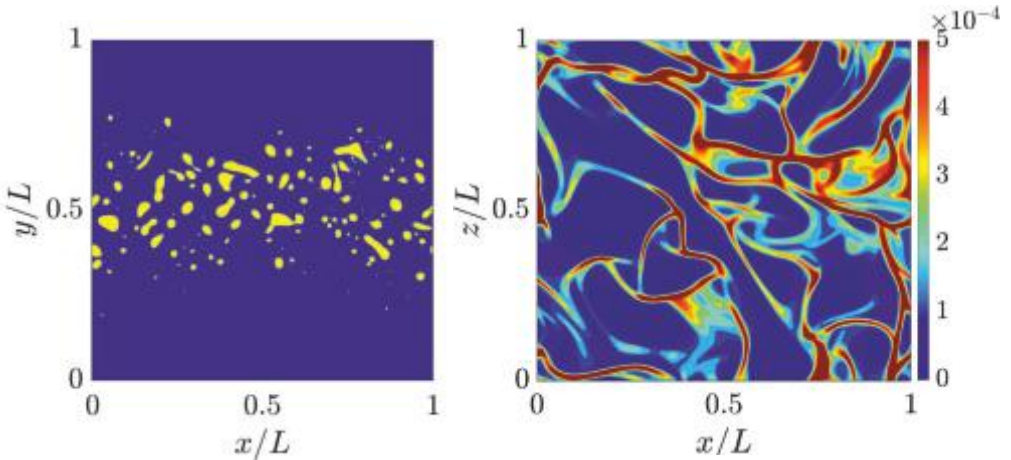
Fig.1: Instantaneous snapshots of the volume fraction at the mid-plane of the periodic box at the latest stages of the decaying HIT for interfacial turbulence (left), and particulate turbulence (right) [1].
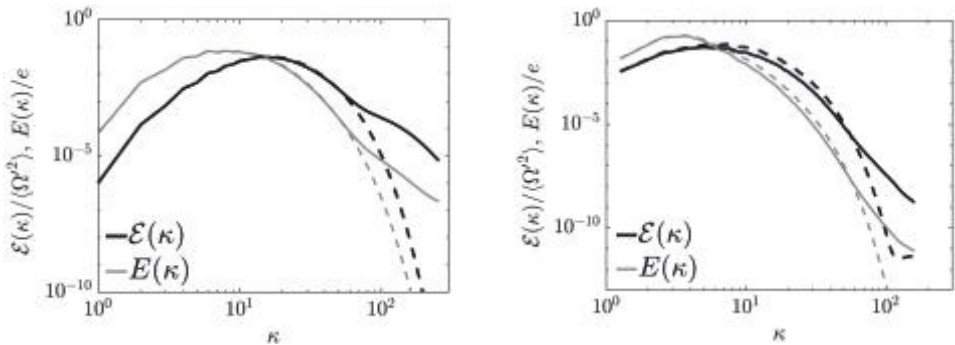
Fig.2: Normalized kinetic energy and enstrophy spectra for the interfacial HIT (left) and particulate-HIT (right) at arbitrary instants of time. Single-phase spectra are plotted in dashed curves.

[1] Saeedipour M., Schneiderbauer S., Toward a universal description of multiphase turbulence phenomena based on the vorticity transport equation. *Physics of Fluids 34, 073317, 2022*.

M. Saeedipour | S. Schneiderbauer

mahdi.saeedipour@jku.at **|** simon.schneiderbauer@jku.at
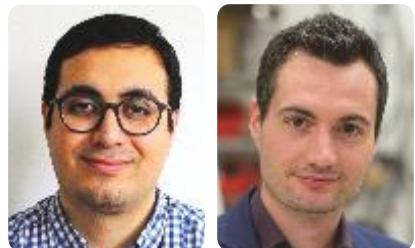
EDITORIAL | MESO

Dear Readers,

Conducting research on the mesoscale means building bridges. Bridges between micro- and macroscopic processes, but also between physically justifiable, accurate models and computational feasibility. Paraphrasing Einstein, we have to make things as simple as possible, but not simpler than that.

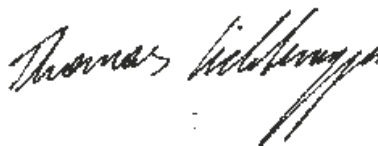Two nice examples are provided by the works of **Tobias Kronlachner** and **Marco Atzori**. Tobias generalized discrete-element contact models such that highly cohesive powders can be simulated if appropriate material parameters are used. Hence, he also had to devise an optimization strategy to find reasonable values without excessive numerical costs as sketched in Fig. 1.

Marco made important contributions to the problem of segregation in polydisperse fluidized beds. He recognized the existence of different time scales between (i) rapid, local, short-term dynamics, (ii) large-scale mass transport and (iii) segregation of different grain sizes, which will allow us to perform data-assisted, fast, long-term simulations. The dynamic regimes of a spout fluidized bed are illustrated in Fig. 2.

I hope that these two teasers have made you curious and that you enjoy reading about our research endeavors.

Sincerely,

Thomas Lichtenegger | thomas.lichtenegger@jku.at

Optimization framework
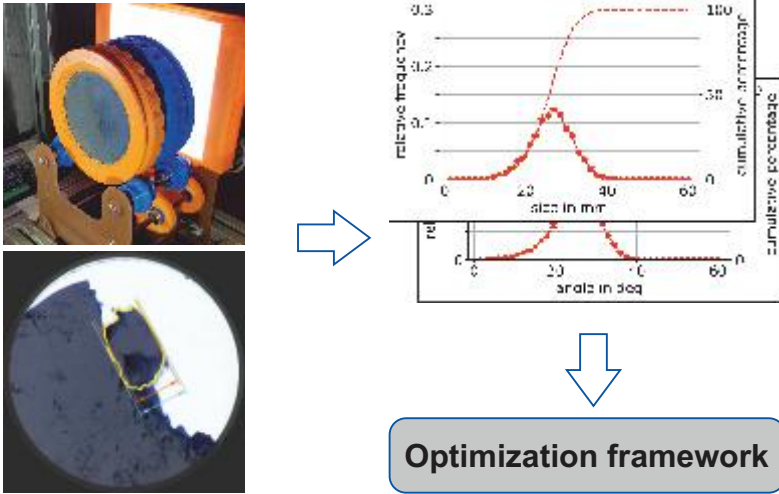
Fig.1: Optimization-based material parameter estimation. The block evaluation results from a rotating drum experiment are used as the target value in the optimization framework to estimate DEM contact parameters with an optimization algorithm.
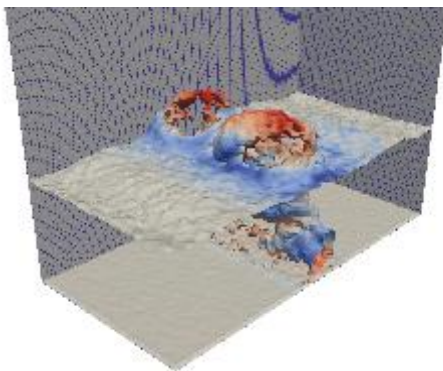
Fig.2: Dynamics of a spout fluidized bed. In the central spout region, particles are strongly fluidized while stagnant zones develop on the sides. This variety of regimes in the same system poses a significant challenge to understand segregation.

MESO | PHYSICALLY-BASED CLOTH SIMULATION

The simulation of cloth is mainly driven by the field of computer graphics to produce visually convincing animations of garments. However, it is also interesting from a more scientific point of view to create realistic descriptions of soft bodies. Not only is cloth modelling helpful to computer-aided design purposes in the clothing and upholstery industry but the same principles are also applicable to simulations of elastic membranes and soft tissue surgery.

Cloth may basically be simulated via continuum methods or using a discrete approach. The latter typically makes use of particles – which represent the crossing points between weft and warp threads – establishing a mass-spring system representing the topology and behavior of a fabric. Provot, for instance, suggested the usage of particles arranged on a square lattice. The fabric is then formed by applying "structural springs" between each particle and its nearest neighbors as well as "shear springs" and "flexion springs" for the next nearest neighbors (Provot 1995).

In this preliminary study we looked at the applicability of the bonded particle model (BPM) to simulations of fabric. The BPM (with some tweaking) has proven to be a versatile tool in our past research activities and has been used to investigate such diverse topics as particle fragmentation and red blood cells. In contrast to Provot's method, we use only a single connection to each particle's nearest neighbors (cf. Fig. 1). Instead of a simple spring, however, the bond connection consists of normal, shear, torsional and bending components.

An interesting aspect when dealing with deformable objects is the potential occurrence of self-collision that must be detected and requires a proper response. Since the fabric consists of densely packed particles in our case, self-intersection is avoided by the repulsive particle-particle interaction forces. No additional measures need to be taken.

Figure 2 shows the simulation results for a square piece of cloth after dynamic draping over different geometric bodies. We note the immediate formation of wrinkling and creasing patterns.

In Fig. 3 we show a setup sometimes used as experimental analogy to gravity wells. A piece of fabric is clamped on a horizontal circular frame. A sphere is placed at the center creating an initial displacement. A second sphere is then added off-center (optionally with a velocity tangential to the frame) and is moving towards the center.
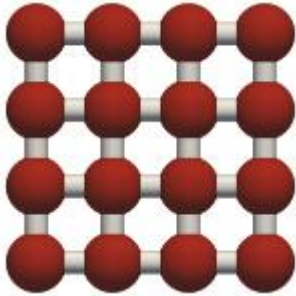

To compare the behavior of a simulated virtual material to an actual fabric one may use a setup similar to the one shown in Fig. 3. The piece of cloth under investigation is clamped on a circular frame (about the size of a mini hula hoop) with as little initial tension as possible. Then a known weight (e.g. a ball or disc) is placed at the middle. We can then measure the displacement of the fabric. Repeating this experiment with different weights we obtain a characteristic force-displacement curve for the material.

Fig.1: Network of bonded particles with each sphere being connected to its four nearest neighbors.
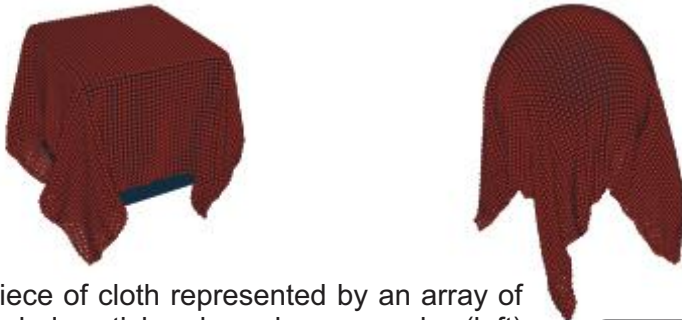

Fig.2: A piece of cloth represented by an array of 81×81 bonded particles draped over a cube (left) and a sphere (right).

Fig.3: Two spheres dropped onto a square piece of cloth (139×139 particles) that is fixed to a circular frame.

Daniel Queteschiner | daniel.queteschiner@jku.at

MESO | MODELING OF FINE COHESIVE POWDERS

Powder metallurgy is essential for producing highly specialized components, such as those for medical diagnostic equipment. The industrially used powders often consist of small, irregular grains, which can cause high cohesive forces between the individual particles. To model the flow behavior of such materials, the discrete element method (DEM), a simulation tool that represents the material by distinct particles, can be utilized. Additional techniques for fine materials are needed to limit the computational cost, which come with the difficulty that the material parameters for the simulation are hard to estimate. We developed an optimization approach based on the block evaluation for the rotating drum experiment. Still, we could not find parameters for a standard model that captured the real-world material's behavior, demonstrated by the block value distribution in Fig. 2 (blue), showing a significant difference for the angle.

This let us conclude that this model is not capable of capturing the blocky behavior of the material. Inspired by a cube rolling on a plane as shown in Fig. 1, we modified the model considering the rolling resistance due to non-spherical particles. With this modification, a significantly better agreement between simulation and experiment could be achieved as visualized in Fig. 2 (green).
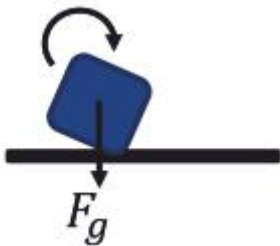

Fig.1: Inspiration rolling cube. Model for the resistance of a cube against rolling.
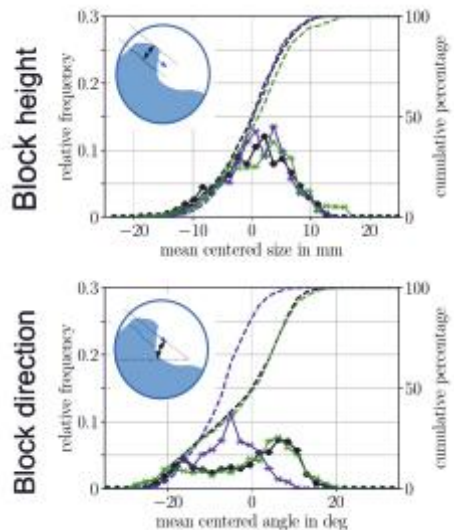

Fig.2: Comparison between simulation and experiment. A subset of block evaluation results for the standard (blue) and the modified model (green) in comparison to the calibration experiment (black).

Subsequently, the estimated material parameters for the specially developed DEM model of strongly cohesive metal powders were used to investigate industrially relevant processes like the filling of a cylindrical die with a filling shoe. A variant of this setup is shown in Fig. 3. One of the key properties is the uniformity of the powder inside of the die after the filling passes. Therefore, we evaluated density to measure its relative distribution in the die geometry. One example of such a density distribution is shown in Fig. 4 where it becomes obvious that there is a significant change along the traveling direction.

Ultimately, our research aims to improve the filling result by changing the filling shoe geometry as well as the moving speed of the shoe during the filling process.

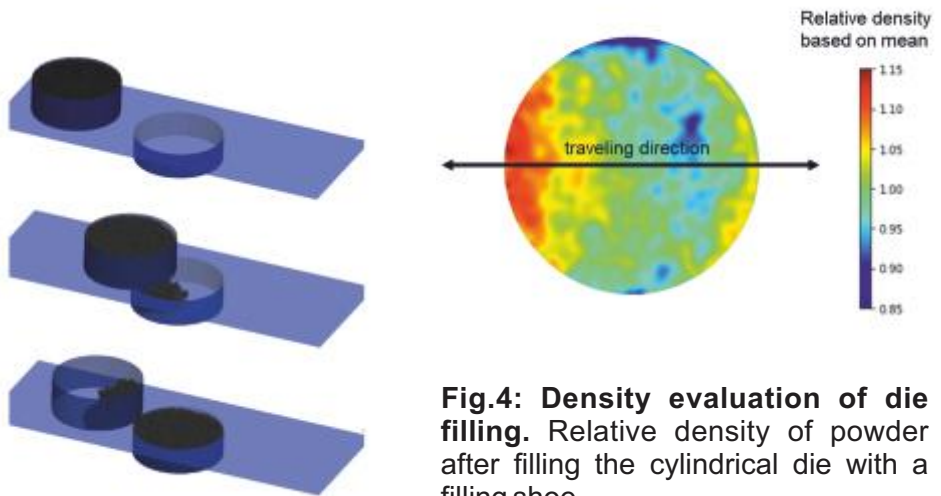**Fig.4: Density evaluation of die filling.** Relative density of powder after filling the cylindrical die with a filling shoe.

Fig.3: Filling process. Filling of a cylindrical die with a cylindrical filling shoe with one forward and one backward pass.

Tobias Kronlachner | tobias.kronlachner_1@jku.at

MESO | SEGREGATION CONTROL IN FLUIDIZED BED

The onset of various degrees of segregation in fluidized beds with spray granulation is an inevitable consequence of the large range of particle diameters resulting from the accretion process. Segregation can negatively affect exposure to spray and lead to unwanted deposition of product, eventually causing a reduction of the process efficiency or requiring maintenance intervention. In principle, it is possible to control segregation in a fluidized bed by modifying the total gas flow, but this operation is often impractical in full-scale plants. The aim of this project is to demonstrate that an air-diverting system can be used to modify the fluidization pattern for a given total flow rate.

Experiments on a full-scale fluidized bed are carried out at TUHH, while CFDEM simulations are performed at JKU to investigate in detail the control effects, using a model test case with a smaller domain size and with a bidisperse particle distribution. Fig. 1 shows the center of mass as a function of time for the two particle classes, in the center and side regions of the computational domain, and for three different inflow configurations with the same total flow rate. In the case with uniform inflow (top panel) the system exhibits long-scale motion and segregation. In the spouted configuration considered here (center panel), *i.e.* when the air-diverting system is set to cause a higher inflow in the center portion of the bed, segregation becomes negligible in the center of the domain. At the same time, the deposition of smaller particles that percolate towards the lower part of the bed leads to an inversion of segregation on the sides of the domain, where the center of mass of the larger particles is higher than that of smaller particles. In an inverse spouted configuration (bottom panel), when air is diverted towards the sides of the domain, the opposite trends are observed. Segregation is apparent only on the side regions, while inverse segregation is found in the center. It is also shown that the non-homogenous aeration in both spouted and inverse spouted cases remove the long time-scale dynamics exhibited by the reference case.
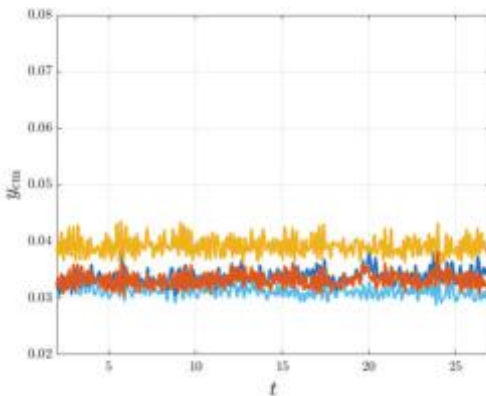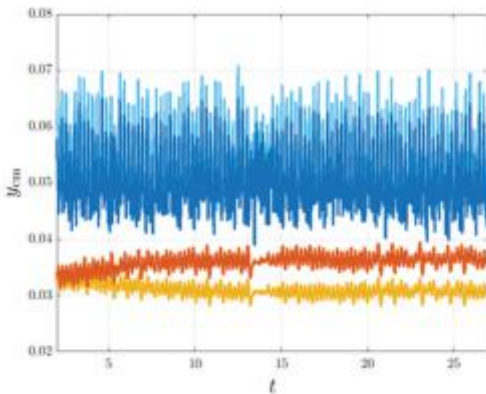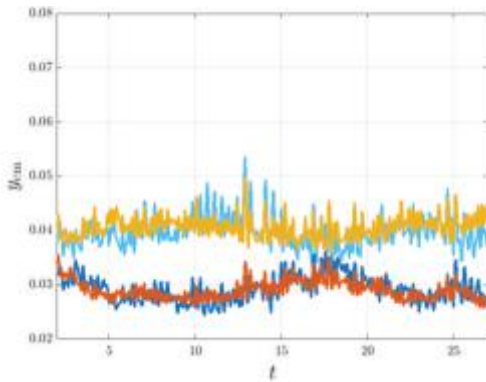
Fig.1: Centre of mass as a function of time for (—) larger and (—) smaller particles in the centre of the bed and (—) larger and (—) smaller particles on the sides of the bed. The three regimes correspond to: **(top)** homogenous inflow, **(centre)** spouted aeration, and **(bottom)** inverse spouted aeration.

Marco Atzori | marco.atzori@jku.at

MESO | IRON ORE REDUCTION: MODEL LIMITATIONS OR PARAMETER UNCERTAINTY

The reduction of ore to iron is a central process in steel-making industry. Regardless if the reaction takes place in a moving (blast or shaft furnace) or in a fluidized bed reactor (FINEX process), the chemistry remains the same: A reducing agent (either CO or H_2) first reacts with hematite, Fe_2O_3, to form magnetite, Fe_3O_4, which is further reduced to wustite, FeO, which finally turns into iron, Fe.

Due to the high energy consumption and carbon footprint (if CO is used as reduction agent), optimization of the full-scale process is a highly desirable goal, which involves a complete understanding of the thermo-chemical state of the whole reactor. However, even though up-scaling and time-extrapolation techniques are continuously developed (both in our group and by others) so that the description of the whole plant will eventually be possible, any such macroscopic simulations are built upon high-fidelity single-grain models. The multi-step reduction described above has inspired a multi-layer shrinking core model of iron ore as shown in Fig. 1. The interfaces between these layers move towards the particle center until one species after the other has been completely reacted.

Although the mathematical formulation of this model is straight forward, it comes with a large number of reaction (kinetic constants) and material parameters (layer porosities, pore diameters). Since literature values are massively scattered, one has to calibrate these parameters for each material. To this end, we use Bayesian optimization so that we find parameters that approximately reproduce well-defined measurements (Fig. 2, left).
Our first results showed some discrepancy with experimental findings, which made us question the validity of the simple multi-layer model. However, these deviations vanished once we allowed for a species-dependent pore structure. Figure 2 (right) shows that the model pictures reality surprisingly well – our initial choice of parameters had simply been too restrictive!
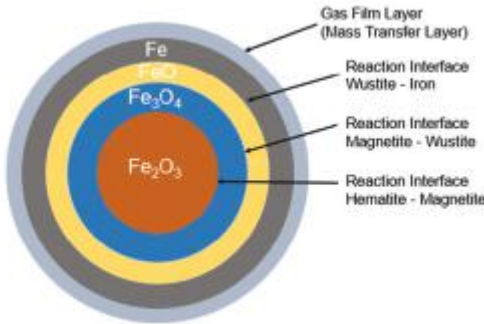
Fig.1: Sketch of the structure of partially reduced iron ore. Layers of different iron oxides develop during reduction from hematite to iron. The reducing agent (CO or H_2) diffuses through pores in the material layers to continue the reaction deep inside the grain.

Fig.2: Illustration of the reduction experiment (left) and the resulting mass loss over time (right). Assuming a constant pore size throughout the particle did not allow to match simulation with experimental results. Layer-dependent pore diameters represented the reduction reaction much more realistically.

Thomas Lichtenegger | thomas.lichtenegger@jku.at

MESO | MODEL AND PERFORMANCE ENHANCEMENTS FOR TRANSPORT BASED RCFD

Simulation of large-scale particle-laden flows is a computational demanding task.
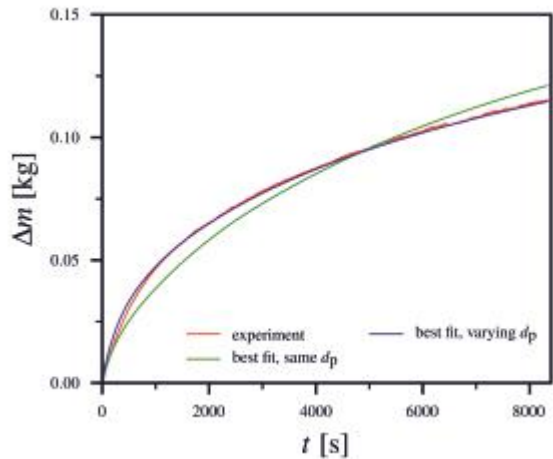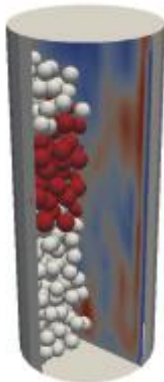While established methods like CFD-DEM coupled method allow such simulations for short time periods, industrial-scale simulations require hours of simulated physical time and therefore some time saving algorithms.

Transport based recurrence CFD (rCFD) is a time extrapolation algorithm, which gives a potential speedup by several orders of magnitude. This allows to simulate spatially large-scale systems of long-lasting passive transport processes.

In this final year of my research project, my aim is to tailor this method to some specific questions of a specific industrial process.

Several details of the algorithm became adapted.
One was the implementation of the Gunn heat transfer model. This model is well established in CFD-DEM coupling methods but require some special considerations for rCFD. I refined the model to enable simulations within the rCFD framework, directly comparable to established CFD-DEM coupled methods.

Another part was to implement several performance improvements. Alterations in data handling, careful selection of utility libraries and proper load distribution to a cluster computer enabled us the simulation of a specific industrial process.
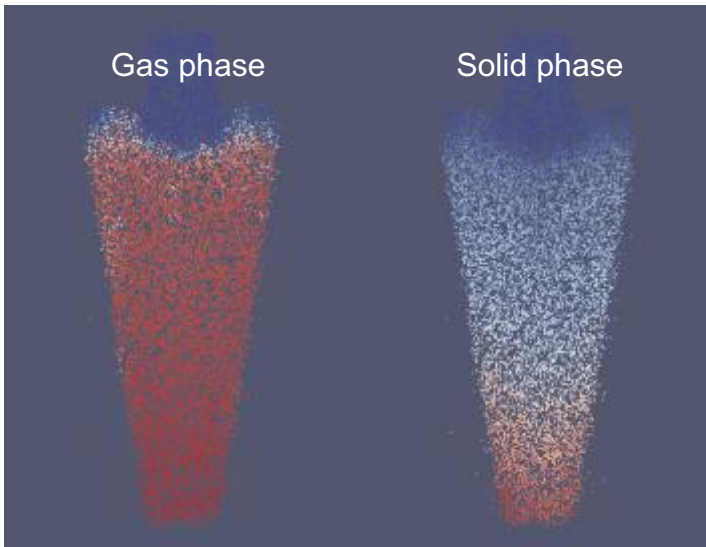
Fig.1: Gunn Heat transfer model on a counterflow hopper as test case. Warm gas is injected from below and heats up the solid phase.

- rCFD run / h
- CFD-DEM run for DB / h
- est. CFD DEM run for comparable simulation / h
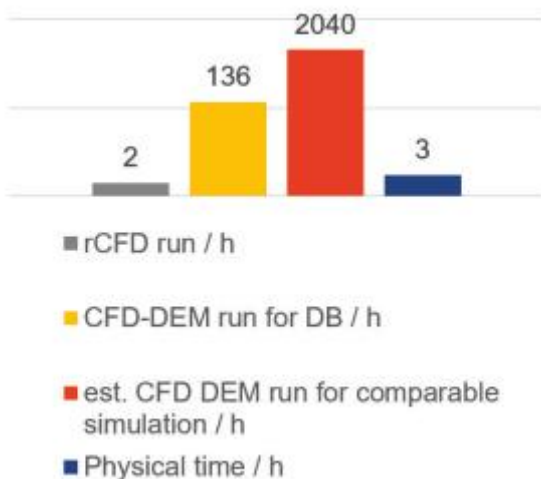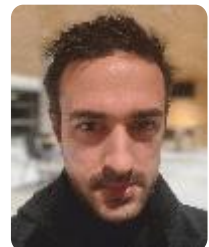- Physical time / h

Fig.2: Performance comparison of industrial case running on 8 CPU cores. Comparing rCFD run and Physical time, rCFD allows faster than realtime simulations.

David Haider | david.haider@k1-met.com

EDITORIAL | MACRO

Dear Readers,

Even though using an appropriate modelling of the impact of the small unresolved scales on the macro-scale, the detailed understanding of these scale might be important for the overall process. Thus, we proposed a concept for a CFD-DEM magnification lens to connect detailed meso-scale simulations of selected sub-regions with coarse macro-scale two-fluid model (TFM) analysis (Fig. 1).

Last year we further released a major update of our OpenFoam solver for large-scale multiphase flows, `twoPhaseEulerTurbFoam`. This update includes the coarse-grid modelling of gas-particle heat transfer (Fig. 2) allowing the analysis industrial-scale fluidized bed reactors.

Additionally, rCFD spreads its applicability towards a variety of disciplines. For example, the transmission of Covid-19 in people gatherings can be effectively pictured by rCFD.

Finally, I want to thank my team members for their encouragement and their excellent work, which has been honoured by high impact Chemical Engineering Science, Physics of Fluids and the International Journal of Multiphase Flow.

Sincerely,

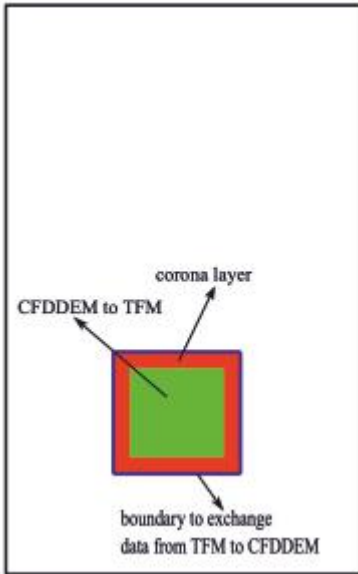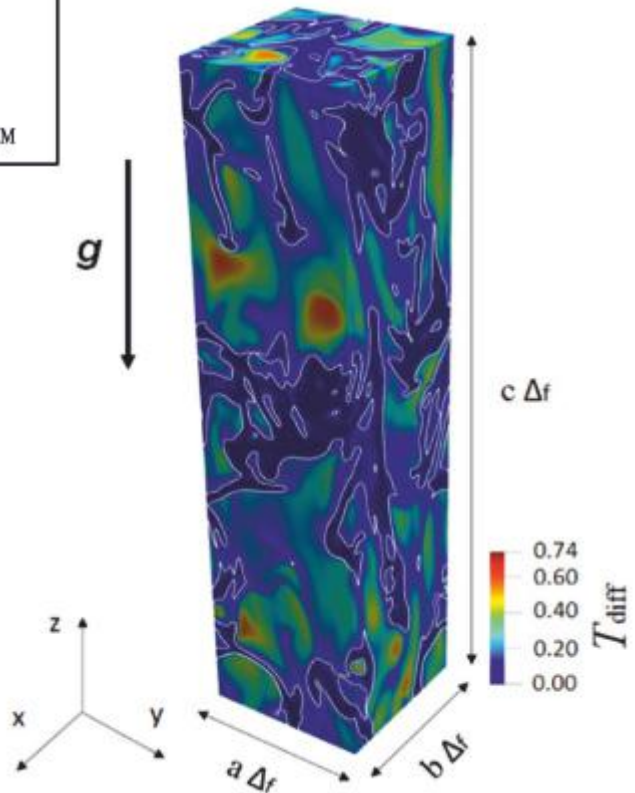**Simon Schneiderbauer |** simon.schneiderbauer@jku.at

Fig.1: Concept for the CFD-DEM magnification lens nested into a coarse TFM simulation.

Fig.2: Temperature difference between gas and particle phases in cluster induced turbulence.
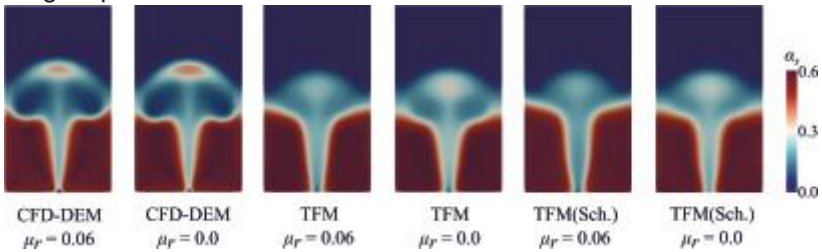
MACRO | TWO-FLUID MODEL AND DISCRETE ELEMENT METHODS IN SPOUT FLUIDIZED BEDS

Spout fluidized beds that combine the favorable properties of both fluidized and spouted beds. This combination enhances particle circulation and mixing as well as a lower total flow rate is needed to fluidize particles in these beds compared to fluidized and spouted beds. Due to the mentioned advantages, the spout fluidized beds have been employed in various processes, including gasification, chemical looping combustion, pyrolysis, and catalytic oxidation. In the past decades, two main modelling approaches including unresolved Computational Fluid Dynamics coupled with Discrete Element Method (CFD-DEM) and Two-Fluid Model (TFM) have been used to analyse hydrodynamics of spout fluidized beds.

In our path through developing a tool to embed unresolved CFD-DEM approach inside TFM, it was of vital importance to have a TFM approach that can anticipate accurate results in comparison with CFD-DEM and experimental data. Therefore, we tried to implement a TFM approach in OpenFOAM. In this TFM approach, the kinetic theory of granular flow used for solving the motion of the solid phase, includes realistic particle-wall boundary conditions for momentum transfer and the flux of pseudo-thermal energy. Frictional stresses in TFM approach were modelled based on a $\mu(I)$−rheology. We proposed a new ad-hoc modification of the $\mu(I)$−rheology to account for the effect of rolling friction (μ_r) in TFM approach.

We applied our TFM and CFD-DEM approaches to simulate single- and multiple-spout fluidized beds. Simulations were validated against the experimental data [1] with four different interphase drag correlations derived from DNS and experiments. Our results showed that there is a good agreement between TFM and CFD-DEM approaches with respect to time averaged volume fraction, solids velocities, solids fluxes and granular temperature.

Particulate Flow Modelling

Single-spout fluidized bed

| CFD-DEM $\mu_P = 0.06$ | CFD-DEM $\mu_P = 0.0$ | TFM $\mu_P = 0.06$ | TFM $\mu_P = 0.0$ | TFM(Sch.) $\mu_P = 0.06$ | TFM(Sch.) $\mu_P = 0.0$ |

Double-spout fluidized bed

| CFD-DEM $\mu_P = 0.125$ | CFD-DEM $\mu_P = 0.0$ | TFM $\mu_P = 0.125$ | TFM $\mu_P = 0.0$ | TFM(Sch.) $\mu_P = 0.125$ | TFM(Sch.) $\mu_P = 0.0$ |

Triple-spout fluidized bed

| CFD-DEM $\mu_P = 0.125$ | CFD-DEM $\mu_P = 0.0$ | TFM $\mu_P = 0.125$ | TFM $\mu_P = 0.0$ | TFM(Sch.) $\mu_P = 0.125$ | TFM(Sch.) $\mu_P = 0.0$ |
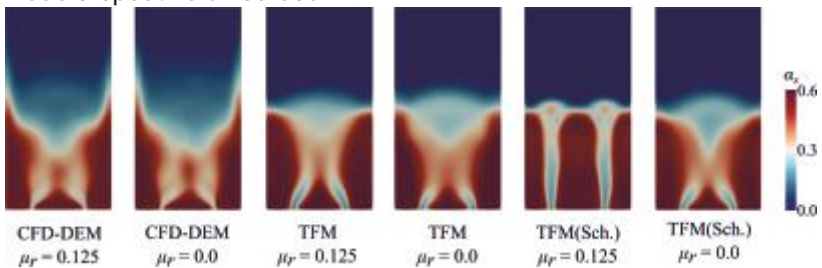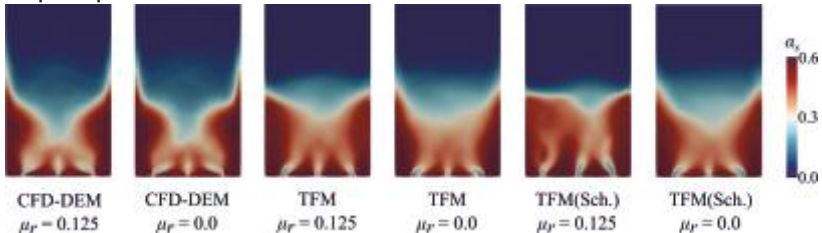
Fig.1: Time averaged solids volume fraction profiles obtained from TFM with Schneiderbauer frictional stress closure [2] (TFM(Sch.)), TFM with Chialvo frictional stress closure [3] (TFM) and CFD-DEM in the single-, double- and triple-spout fluidized beds.

[1] Van Buijtenen, M.S. et al., 2011. Numerical and experimental study on multiple-spout fluidized beds. *Chemical engineering science*, *66*(11), pp.2368-2376.
[2] Chialvo, S., Sun, J. and Sundaresan, S., 2012. Bridging the rheology of granular flows in three regimes. Physical review E, 85(2), p.021305.
[3] Schneiderbauer, S. et al., 2012. A comprehensive frictional-kinetic model for gas–particle flows: Analysis of fluidized and moving bed regimes. Chemical Engineering Science, 80, pp.279-292.

Behrad Esgandari | behrad.esgandari@jku.at

MACRO | A COARSE-GRID CFD SOLVER FOR FULL-SCALE GAS-PARTICLE FLOW REACTORS

Moderately dense gas-particle flows play an important part in many industries, not just chemical engineering. Commonly, there is a large difference in size between the particle diameters (a few micro-meters) and the reactor dimensions (tens of meters). Thus, numerical simulations, which resolve all forces acting on this huge number of particles are not feasible, not even on current supercomputers. Therefore, we developed a solver for fast and reliable prediction of the macro-scale flow properties, such as solid volume fraction and temperature distribution, in real-scale gas-particle flow reactors.

The solver is based on spatial filtering of the Two-Fluid Model balance equations, which describe both phases as continua. Thereby, the unresolved contributions in coarse-grid simulations stemming from unresolved meso-scale structures, such as particle clusters, are modelled. In particular the exchange term correlations for momentum and heat need to be corrected. We found that the resolved drag force and heat transfer can be corrected by constructs called the drift velocity and drift temperature, these are measures for the meso-scale heterogeneity of the flow. The drift temperature, for example, represents the gas-phase temperature fluctuations seen by the particles. We used a test-filtering approach together with transport equations for the variances of the variables to calculate the drift velocity and temperature locally and dynamically during the course of coarse-grid simulations. As can be observed in Fig. 2, this dynamic approach yields excellent predictions for the sub-grid variables, and, consequently, for the macro-scale flow properties. As an example, the predicted temperature distribution in a fluidized bed is shown in Fig. 1.

The developed solver is implemented in OpenFOAM, based on the Two-Fluid Model solver twoPhaseEulerFoam. It is available on github at github.com/ParticulateFlow/pfmFOAM-public supported by some tutorial cases.
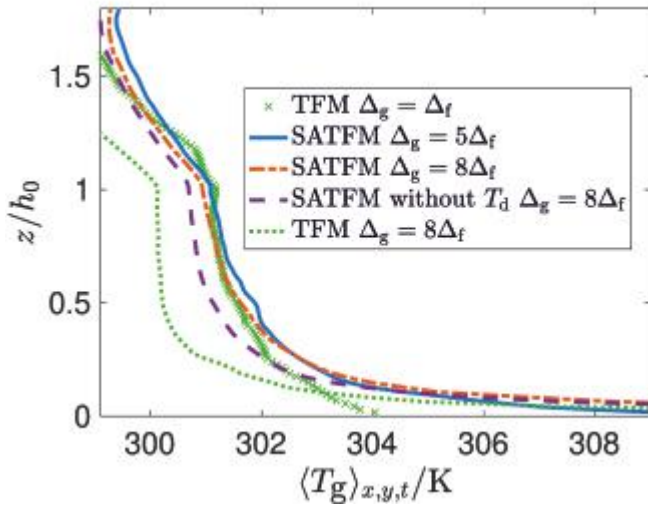
Fig.1: Time-averaged gas-phase temperature distribution over the height in a fluidized bed after 5 seconds, where the inflowing gas temperature was elevated from 300 K to 800 K during the time between 3 and 4 seconds. The developed solver (SATFM) yields good agreement for differently coarse grid sizes, while the TFM fails on the coarse grid in comparison with fine-grid TFM reference data.

Fig.2: Dynamically calculated drift temperature in comparison with fine-grid reference.

Stefanie Rauchenzauner | stefanie.rauchenzauner@jku.at

MACRO | ANISOTROPY CHARACTERIZATION OF TURBULENT FLUIDIZATION

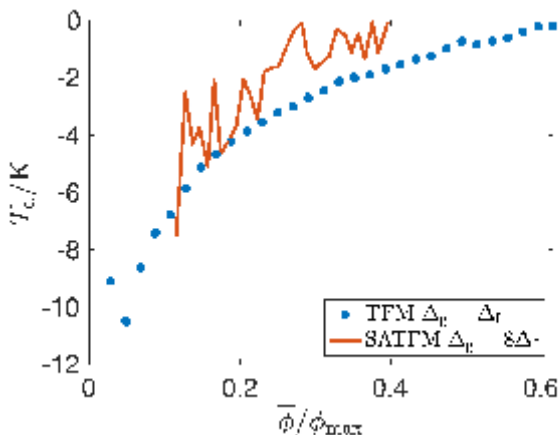What is the structure of turbulence in moderately dense gas-particle flows? Is there a return-to-isotropy phenomenon in multiphase flows such as observed in turbulent single-phase flows? These and many more research questions were studied to unveil the characteristics of turbulent gas-particle flows.

Based on highly resolved kinetic-theory-based two-fluid model simulations of turbulent fluidization (figure 1), the phase-filtered anisotropic Reynolds stress tensor is considered to classify the possible states of turbulence in the barycentric anisotropy invariants map (figure 2). Analyzing the joint probability density function (JPDF) of the Reynolds-stress clearly shows that in gravity driven gas-particle flows turbulence is highly anisotropic showing a predominant contribution in the direction of gravity (Figure 3). Nevertheless, these one-dimensional structures tend to move always towards isotropy, revealing the return-to-isotropy problem and the tendency to extinguish the bulk anisotropy.

Furthermore, our analysis shows that the granular temperature as a quantitative measure of uncorrelated particle agitation responsible for particle collisions is found to accumulate predominantly in this 1-D turbulence region.

This findings are especially important for the further development of multiphase turbulence models. Future work will concentrate on the analysis of the appropriate structural predictions of multiphase turbulence models.

Dabbagh, F., Schneiderbauer, S. (2022). Anisotropy characterization of turbulent fluidization. Physical Review Fluids, 094301.
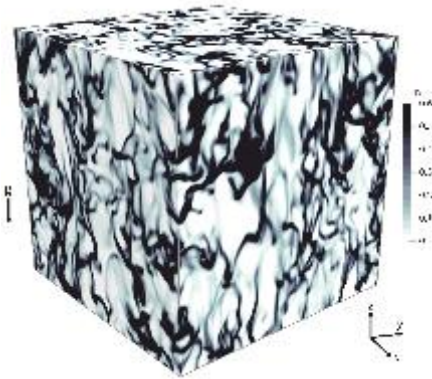
Fig.1: Clustering in a turbulent gas-particle flow.

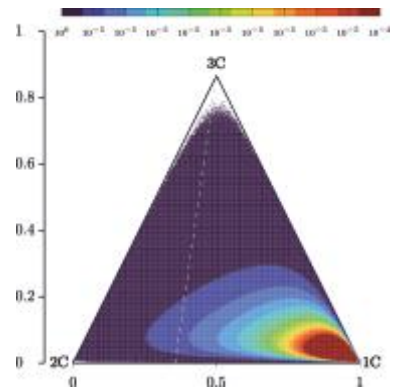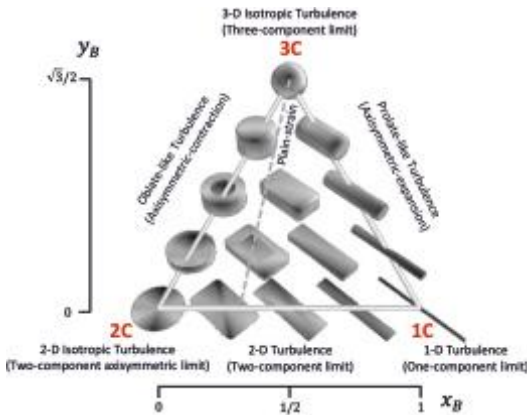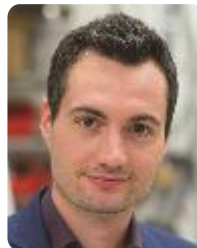**Fig.3:** Joint probability density function of the Reynolds-stress.

Fig.2: Barycentric anisotropy map (BAM) used to analyse the anisotropy of turbulence.

Simon Schneiderbauer | Firas Dabbagh

simon.schneiderbauer@jku.at **|** firas.dabbagh@borealisgroup.com

MACRO | DEFLAGRATION

Deflagration describes the very fast and typically uncontrolled as well as undesired combustion of dust particles levitated in gas flows. Consequently, any deflagration event is closely coupled to the characteristics of the fluid-dynamical behaviour of dust particles. Deflagration is particularly important for the safety of different industrial processes including fine dusts.

With joint efforts together with Hoerbiger GmbH and the Montan University Leoben, we thoroughly study deflagration events of organic dusts following a threefold research strategy (i.e. theoretical, numerical and experimental investigations).

Numerically, we employ a Euler-Lagrangian method, where the trajectories of the dust particles are tracked by representative parcels. Since the combustion of dust particles involves relatively high temperatures radiation has to be considered, which is especially important for the particle-particle heat transfer and the ignition using electric sparks.

Finally, first comparisons of the predicted particle temperatures with experimental observations of dust deflagration events in a modified Hartmann tube (fig. 1) reveal fairly good agreement the flame speed and its form. Further efforts have to be put on developing new postprocessing routines to allow detailed comparisons of the numerical simulations with experiments to verify the degree of clustering and combustion temperatures.
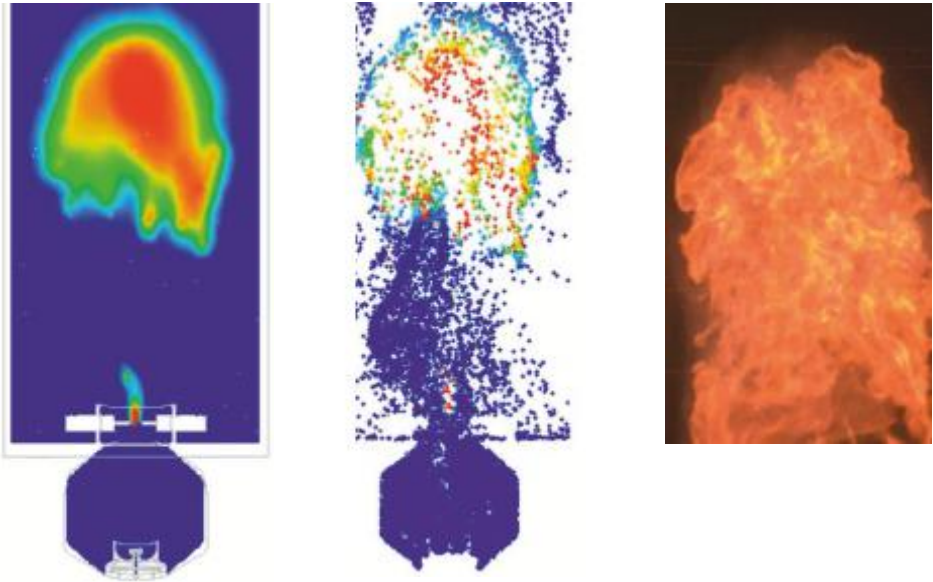
Fig.1: Comparison predicted combustion pattern with experiments (blue: 300 K; red: 2000 K) for a deflagration event of maze starch particles-gas mixture in the modified Hartmann tube.

S. Puttinger | S. Schneiderbauer | S. Pirker | C. Spijker

Stefan Pirker | stefan.pirker@jku.at

MACRO | DATA-BASED RECURRENCE CFD TO STUDY SOLID MIXING INDEX PREDICTION IN LAB-SCALE AND PILOT-SCALE FLUIDIZED BEDS

The multiphase simulations of gas-solid fluidized beds are limited to short durations, because they are computationally expensive and requires huge simulation support. This has made the gas-solid process too slow in order to picture particle conversion or heating of solid. Simulations of highly complicated industrial-scale flows, such as polymerization in fluidized beds or steel refining in gas stirred vessels, are possible because of dedicated at-present multi-phase models. In order to efficiently time-extrapolate long-term processes, data-based recurrence CFD stands as a potential candidate to simulate gas-solid mixing, particle conversion, heating of solid with full CFD resolution. In order to simulate these processes without loosing the spatial resolution, we further develop data-based recurrence CFD to capture secondary gas mass discharge and solid mixing behavior with comparison towards classical Two-Fluid Model (TFM) based full CFD simulations for fluidized beds.

We focused on studying gas-solid mixing on both lab-scale and pilot-scale fluidized beds. We applied different sequence stitching patters, with negative diffusion coefficient in order for the solid particle to fully mix within short time. As can be seen in Figure 1, the evolution of secondary gas mass doesn't comply with classical full CFD simulations for lab-scale, whereas the mixing and gas mass are mostly accurate and comply with full CFD results. The concentration of cells is densely accumulated at the output, which results in the peak curve during the end of iteration, and should be calibrated with the negative diffusion term. As can be seen from both results, the solid mixing tends to show different behavior even though they are simulated with same Δt and other parameters. Figure 2, shows the snapshot of solid mixing for lab-scale and pilot-scale for extrapolation mode. The simulations times were reduced by more than two orders of magnitude (10,000 times for lab-scale & 30,000 times for pilot-scale), capable of matching up to real-time.

We will further investigate the behavior of solid mixing in lab-scale and pilot-scale fluidized bed, with varying boundary conditions. Finally, we apply rCFD to study gas-solid mixing and heating for industrial-scale fluidized bed at P&G Ltd, Newcastle.
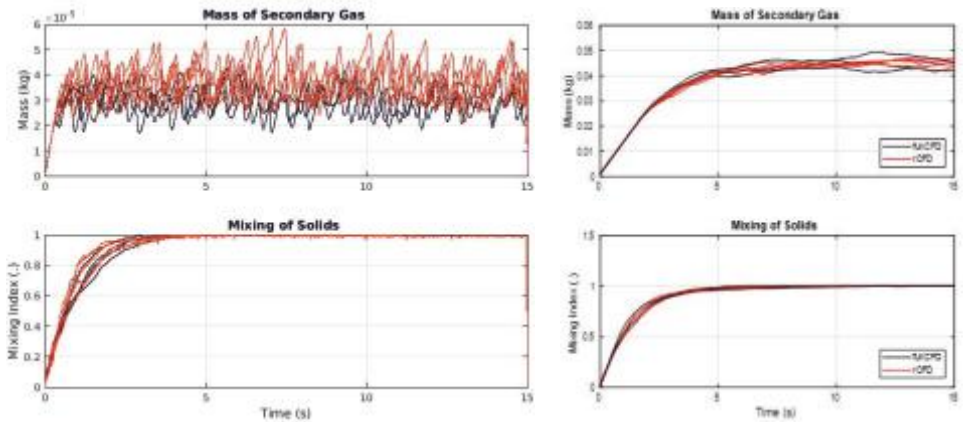
Fig. 1: Evolution of the secondary gas injection and solid mixing predicted for injecting 1tracer/cell throughout the computational domain for lab-scale and pilot-scale.
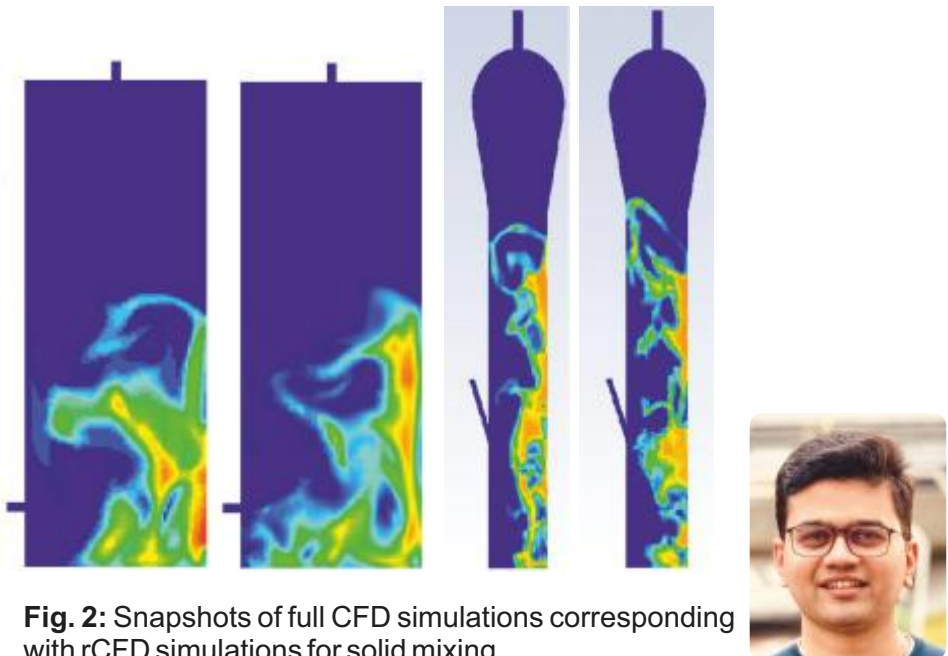

Fig. 2: Snapshots of full CFD simulations corresponding with rCFD simulations for solid mixing.

Varun Dongre | varun.dongre@jku.at

MACRO | RECURRENCE CFD

In the last couple of years we have successfully applied data-based rCFD to e.g. solid mixing and heat transfer in gas-solid fluidized beds. However, in all these simulations we stuck to strictly mono-disperse particle ensembles.

While it would be straight forward to just passively trace particle size information, this wouldn't represent the core physics of poly-disperse fluidized beds. In mildly bubbling fluidized beds larger particles tend to accumulate in the lower region of the bed, while smaller particles will preferentially find themselves close the bed's freeboard. This phenomenon of size-dependent particle de-mixing is called segregation. At process scale, segregation might eventually lead to de-fluidization of the larger particles.

In order to consider segregation phenomena in mildly ploy-disperse particle ensembles, we have to distinguish between the mean flow patterns (of all particles together) and the individual fractional flow patterns. While the bulk of all particles will follow the mean flow pattern, larger particles will experience a superposed drift in downward direction (smaller particles vice versa in upwards direction).

In the realm of rCFD simulations, we account for these fractional flow deviations by introducing a size dependent drift velocity. For the sake of simplicity we define this drift velocity just in vertical direction and we adjust its magnitude by the difference between the fractional diameter and the global Sauter mean diameter of the solid inventory. Technically, we implemented this additional fractional drift by means of face swaps.

In figure 1, we see the evolving vertical mean coordinates of the bulk solid together with those of small and large particle fractions, while in figure 2 corresponding vertical profiles are given. Despite its simplicity, our adapted rCFD simulations seem to be able to reproduce reference CFD-DEM simulations very well.

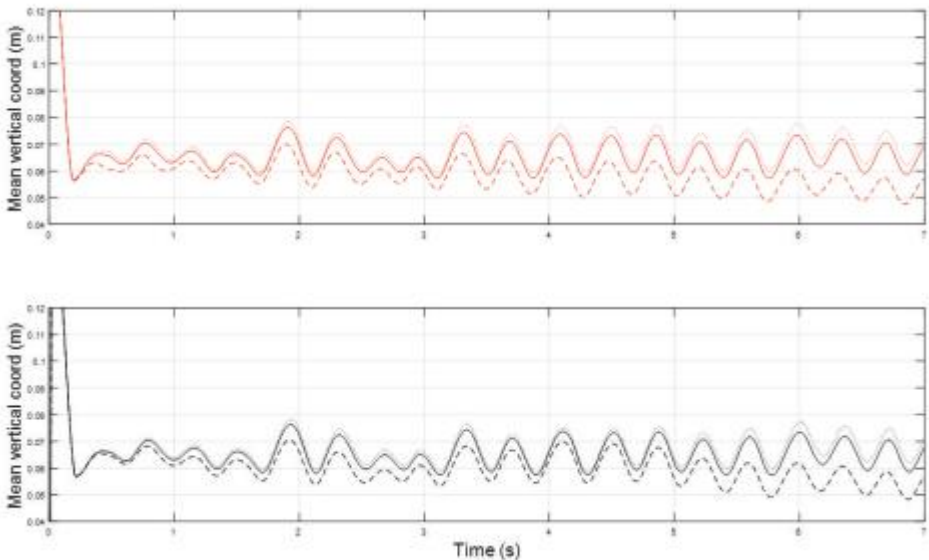**Fig. 1:** Time evolution of vertical mean coordinate of large (dashed lines) and small (dotted lines) particles, (red) rCFD simulations are opposed to (black) full CFD-DEM reference simulations.
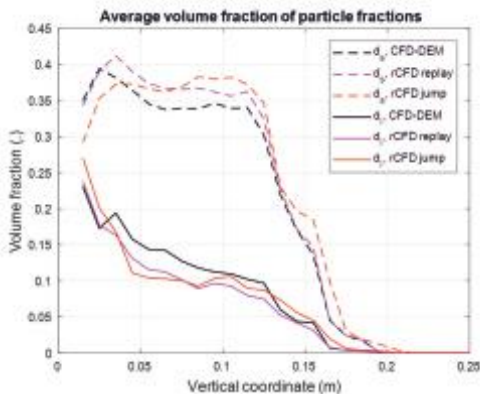

Fig. 2: Vertical profiles of fractional volume fraction of (solid lines) large and (dashed lines) small particles depicting significant segregation.

Marco Atzori | Stefan Pirker

marco.atzori@jku.at **|** stefan.pirker@jku.at

EDITORIAL IV
EXPERIMENTS & DATA ANALYSIS

Dear Readers,

the past year was very challenging for experimental work – while planning our activities for the upcoming years we realized that we will run into a serious lack of space in our lab. After some internal discussion we came to the conclusion that after 12 years of successfully operating our fluid mechanics laboratory at JKU it would be time to make a major investment in our future experimental activities and initiate a fundamental reconstruction of our lab. This lead to an extension of the intermediate floor to provide extra space and the installation of an enclosed measurement room for laser operations (**Fig.1**).

While the construction work was going on, the experimental activities at JKU were obviously limited. Fortunately, one of the major experimental projects in 2022 was located not in-house but at the Montanuniversität Leoben, where we successfully conducted several test series on organic dust deflagration in cooperation with the Chair of Thermal Processing Technology (**Fig.2**). In fact, these tests have not been the only measurement campaign in Leoben last year. The COMET program provides a fruitful framework for cooperation between academic and industrial partners and one of our K1Met projects provided the opportunity to conduct experiments together with colleagues at RHI- Magnesita (c.f. page 48).

Sincerely,

Stefan Puttinger

Stefan Puttinger | stefan.puttinger@jku.at

(a) Oops, somebody cleaned the lab – who said there is a lack of space?

(b) Since there is no direct access to our lab to bring in heavy loads, we had to move in every piece by hand.

(c) Timberwork

(d) The new 'dancefloor' upstairs – 90m^2 of additional space.

(e) Reorganized ground level of the lab with the new laser room on the right.

Fig.1: Some impressions from the lab reconstruction made during summer 2022.
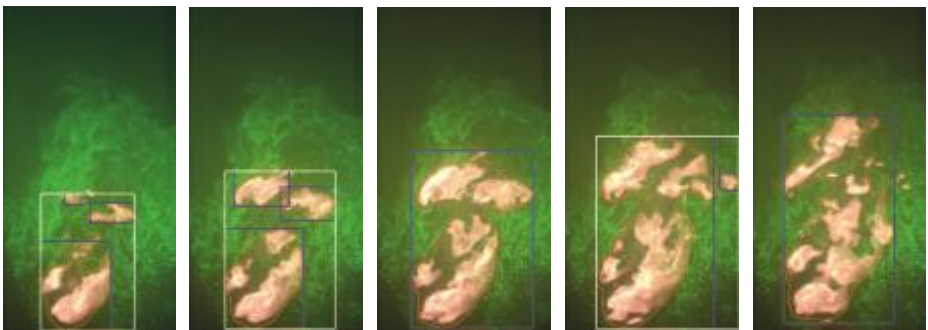

Fig.2: Propagation of a dust deflagration in a cloud of corn starch illuminated by a laser light sheet. The particle concentration is close to the minimum concentration for deflagration. Hence, we see only confined reaction zones that move slowly through the particle cloud.

EXPERIMENTS & DATA ANALYSIS
DUST DEFLAGRATION

When handling organic or metallic powders dust explosions are likely to occur as soon as a few basic requirements are fulfilled: (i) a sufficient mass fraction of fines, which is specific to the substance, (ii) the presence of oxygen or other oxidants and (iii) an ignition source is present that exceeds the minimum ignition energy (MIE) of the material (**Fig.1**).

Standardized test devices like the Hartman tube or the 20l SIWEK apparatus are either not optically accessible or represent bounded flow conditions. To validate numerical modelling activities we have set up a test rig that provides deflagration conditions under low wall influence (**Fig.2**). The major novelty in this test system is the usage of a laser illumination for the particle cloud. This allows to visualize the dust cloud and the reaction zone during the same experiment with identical camera settings. A color high-speed camera is used to record the experiments and a sophisticated image processing then allows to separate the dust cloud and the flame area and calculate macroscopic values like the flame area and propagation velocities but also locally resolved velocities of the dust cloud. To obtain consistent results for different reaction conditions (c.f. the deflagration example with low dust concentration on the previous side and the example in Fig.1), we make use of machine learning based techniques like k-means clustering for image segmentation and neural network based optical flow calculation.

Figure 3 compares the average and maximum vertical flame propagation velocities for different amounts of corn starch. Above a certain minimum dust concentration, flame expansion takes place at velocities in the range of 3 to 7 m/s. The black error bars also indicate that the repeatability of the experiments is very good.

The experimental results have recently been condensed to a journal paper and submitted to Powder Technology.
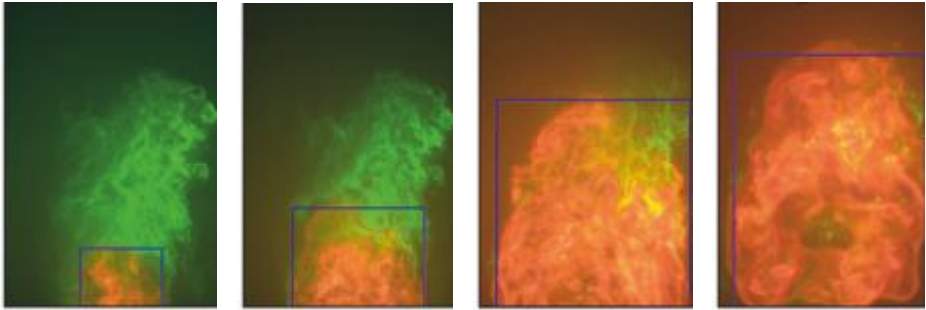
Fig.1: Image series of a dust deflagration experiment. A k-means clustering method is used for image segmentation and allows to extract the boundaries of the dust cloud and flame very accurately. The red line in the examples are the calculated boundaries of the flame and their bounding boxes (blue) to calculate the vertical expansion velocities.
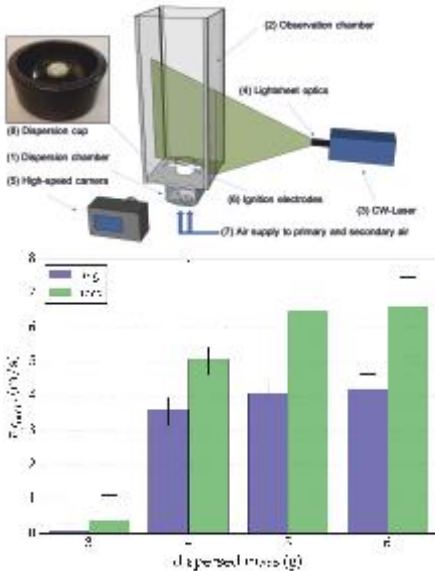

Fig.2: Innovative experimental setup based on laser illumination and a high-speed color camera to measure dust cloud and flame propagation during the same experiment. A color space transformation allows to separate the particles and the reaction zone to calculate spatial and temporal evolution during dust deflagration.

Stefan Puttinger | Christoph Spijker

Fig.3: Influence of particle mass on the averaged and maximum flame propagation velocities during the first 100 ms of the deflagration event.

Stefan Puttinger | stefan.puttinger@jku.at

EXPERIMENTS & DATA ANALYSIS
VORTEX FORMATION AND DROPLET ENTRAINMENT

The entrainment of non-metallic inclusions is triggered by three major mechanisms: (i) shear forces at the interface, (ii) bubble induced entrainment due to argon injection and (iii) vortex induced entrainment. For the latter we have set up a simplified test rig to test the boundary conditions so that droplet entrainment occurs. Water is injected tangentially in a cylindrical vessel to enforce a rotating flow. The outlet is located centrally at the bottom. The water is covered with an oil layer of constant thickness but various viscosity of the oil (**Fig.1**). For such a two-fluid system the driving parameter for the vortex entrainment is not the surface tension of oil or water, but the interfacial tension between these two liquids. Since this interfacial tension is lower than the surface tension for water and air, the entrainment of droplets actually starts earlier for the two-fluid case compared to the case of water and air only. The interfacial tension needs to be determined experimentally for every combination of liquids.

Figure 1 shows that the wavelength of the interface instability changes significantly with the interfacial tension and viscosity of the fluids. Also the shape of released droplets changes and results in elongated filaments for oil with a viscosity lower than water (**Fig.2**).

In a second experiment we built a downscaled continuous casting mold with submerged entry nozzles (SEN) that only have an outlet port on one side to enforce asymmetric flow conditions around the SEN at the interface level (**Fig.3**). The mold also has additional inlet nozzles on the narrow sides to influence the flow velocities around the SEN and thus, the occurrence frequency of lee side vortices. Image processing allows to identify vortex and droplet entrainment for different flow conditions.

The major goal of this studies would be to identify the significant scaling parameters to transfer the results of such water-oil experiments to the real steel-slag system. Since measurements in the real casting mold are hardly possible and available material properties like the slag viscosity have a high uncertainty, there is still no universal solution to this scaling problem.
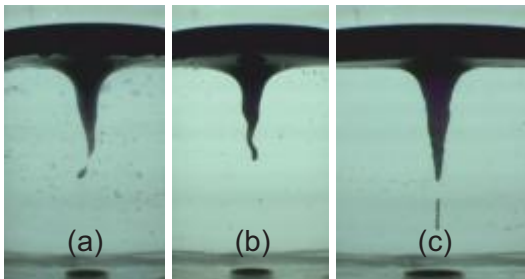
Fig.1: Vortex entrainment and interface instability in a cylindrical tank with tangential flow inlet. The covering oil has a kinematic viscosity of (a) 500 m2/s, (b) 50 m2/s and (c) 0.65 m2/s.
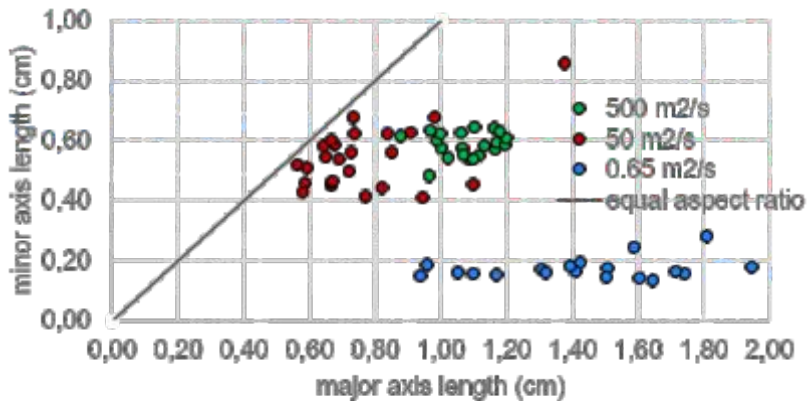

Fig.2: Aspect ratio of the released droplets for different oil viscosities.

Fig.3: Vortex triggered droplet entrainment around a submerged entry nozzle in asymmetric flow conditions.

Stefan Puttinger | stefan.puttinger@jku.at

EXPERIMENTS & DATA ANALYSIS MICRO-DROPLET GENERATION IN MARANGONI FLOW

The evolution of a single droplet deposited onto a liquid surface has experienced increasing attention since numerous applications in chemistry, biology and life sciences can benefit from controllable and reproducible flow patterns on a microscale. In binary fluids of different surface tension, the Marangoni effect is the main driving force of fluid motion and can it can be used to produce micro-droplets.

Figure 1 shows an example of such a system where a droplet of water mixed with 35 wt.% of isopropyl alcohol is deposited on sunflower oil. The drop has an initial size of approx. 5mm in diameter and immediately starts to spread outwards. On its outer boundary the droplet forms a very thin layer which eventually encounters an instability regime at a certain radius (bursting radius r_B) where fingers of a typical distance λ are formed. These fingers periodically release droplets which are spreading outwards while decreasing in size until they reach a maximum extent at the spreading radius r_S.

From the zoomed areas in **Fig. 2** we see that the size of the satellite droplets is not constant. The initial size is related to the fingering wavelenght λ and the thickness of the fingers. However, there seems to exist a maximum size $d_{sd,max}$ for the largest fingers. On their way outwards the satellite droplets shrink until they reach their minimum droplet size $d_{sd,min}$ and gather at the maximum spreading radius r_{smax}. The size range of satellite droplets between $d_{sd,max}$ und $d_{sd,min}$ strongly varies with alcohol concentration. **Fig. 3** shows the correlation of the maximum initial droplet size $d_{sd,max}$ with the wavelength λ, where both values have been normalized with the bursting diameter d_B.

Further research will focus on the decrease in diameter of the droplets when spreading outwards to the gathering radius r_S. Since the generated droplets are very small for higher concentrations of alcohol, a higher image resolution is needed to obtain reliable data for the droplet size distribution as a function of time, radius and alcohol concentration.
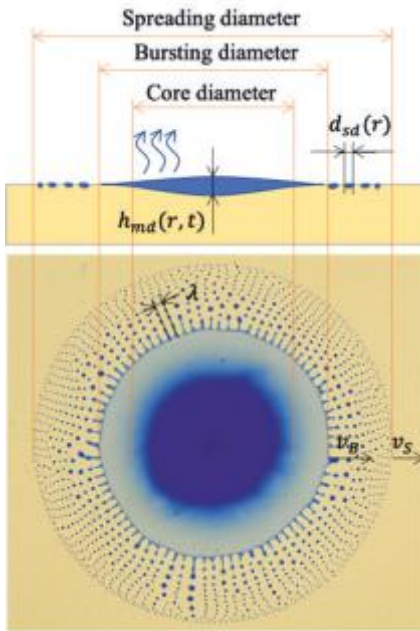
Fig.1: Droplet of water-alcohol mixture on sunflower oil showing the main properties of interest.
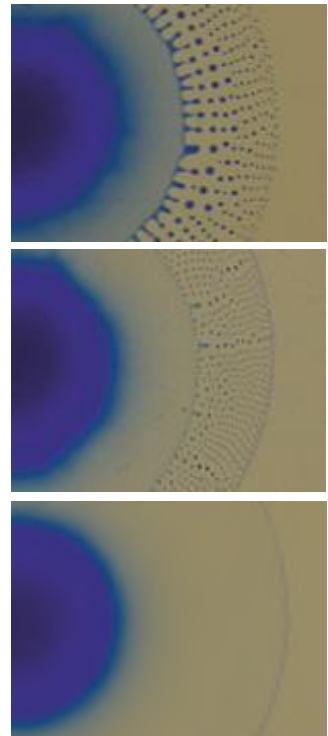

Fig.2: Droplet topology 2s after release for (a) 35, (b) 45 and (c) 55 wt.% of alcohol.
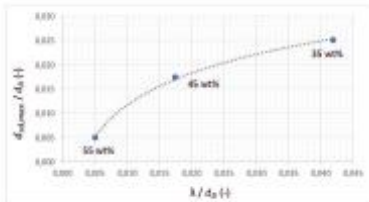
B. Esgandari | T. Kronlachner | S. Puttinger

Fig.3: Maximum satellite droplet size $d_{sd,max}$ as a function of the fingering wavelength λ relative to the bursting diameter d_B.

behrad.esgandari@jku.at | tobias.kronlachner@jku.at | stefan.puttinger@jku.at

EXPERIMENTS & DATA ANALYSIS
INSTABILITIES IN MASSIVE GAS INJECTION

Gas injection into tanks filled with liquid shows an instability pattern that leads to the collapse of the low density area (the gas jet) and causes local backflow of liquid towards the inlet nozzle. Such injection conditions can be found for example in steel ladles. The local backflow may cause additional wear to the nozzles and the lining of the ladle. The frequency of such backattacks has an inverse correlation with the flow rate of gas injection (**Tab.1**). For high flow rates the instabilities decrease, but the inertia of backflow increases. To support Mahdi's modelling activities to simulate gas injection at high flow rates, we organized a test campaign at the laboratory of RHI-Magnesita in Leoben (**Fig.1**). **Figure 2** exemplarily shows an image series of a test with 200l/min injection rate. The images cover a time span of approx. 300 ms and the red lines roughly indicate the topology changes in the gas-liquid interface. At the beginning of a backattack event the interface starts to oscillate until the jet finally narrows to zero and the remaining air pocket further shrinks and induces a backflow towards the nozzle. The jet then needs a few attempts to intrude into the liquid to its original penetration depth. Although it is not possible to visualize shock waves we could qualitatively demonstrate what happens and support the physical understanding of the problem.
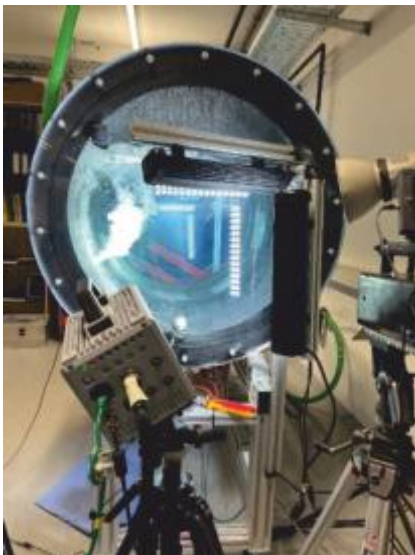

Table 1 Number of backattacks within 5 min of measurement time for different gas injection rates.

flow rate (Nl/min)	number of backattacks
75	1180
100	317
125	182
150	56
175	32
200	17

Fig.1: Test setup with a high-speed camera and LED light-bars at the laboratory of RHI-Magnesita in Leoben.
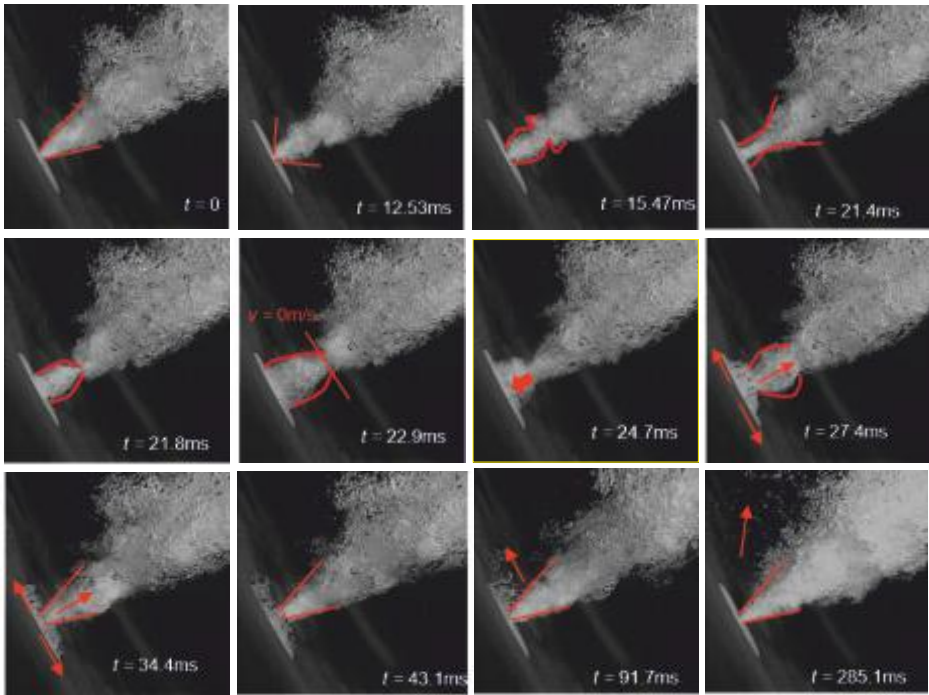
Fig.2: Images of a high-speed video of 200l/min air injection into the water tank of Fig. 1. The recording rate was set to 15.000 frames per second.

Stefan Puttinger | stefan.puttinger@jku.at

EXPERIMENTS & DATA ANALYSIS
LONG TERM STATISTICS OF BLAST FURNACE RACEWAY MONITORING

In the previous funding period of K1Met we developed a tuyere blockage detection algorithm that is based on the hot wind pressure data. The procedure has been implemented in the process control system at voestalpine Donawitz in 2019 and is recording data since then. As a result, we now have several years of operation data available that provides a good basis for long term statistics and to analyze the event history of individual tuyeres ahead of their damage.

Table 1 shows the number of recorded blockage events per day and tuyere for the years 2019 to 2021. The long term data makes clear that the number of raceway blockages is not constant over time but typically influenced by several parameters like the available burden material and the used charging patterns. BF 1, for example, shows a decrease in the number of raceway blockages to almost half the number in 2021 compared to 2019.

The collected data also allows to correlate the tuyere lifetime with the number of blockage events and their severity. In **Fig. 1a** we see that tuyeres that have been replaced in a regular maintenance without a damage follow a linear correlation of events during their lifetime (blue dots). In contrast, damaged tuyeres often show a significant higher number of recorded events (orange dots). Only tuyeres with a very short lifetime can not be distinguished from undamaged tuyeres. So these damages might have various other reasons. **Figure 1b** shows the correlation of the cumulative event strength and the number of events per day. Again, this data follows a linear trend and undamaged tuyeres all lie in a narrow region (indicated by the red line), while damaged tuyeres show a wide spread of events strength vs. event number.

The next steps will be to implement a maintenance indicator to predict the tuyere lifetime and verify this parameter on the available data.
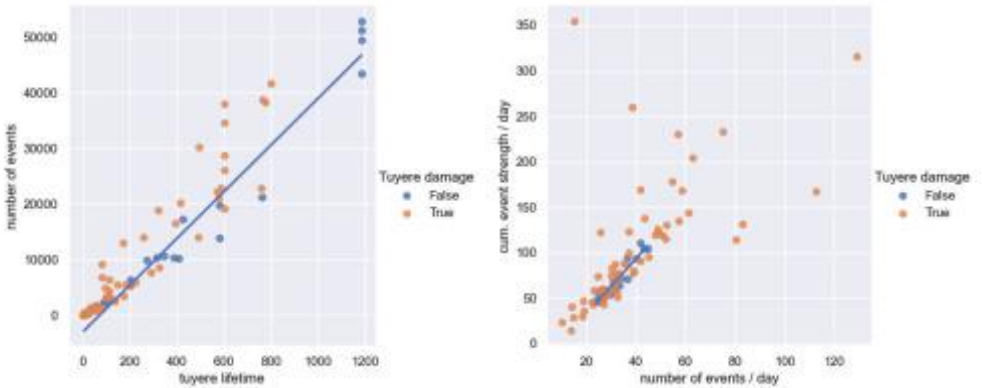
Fig.1: (a) Correlation of the number of blockage events and the tuyere lifetime and (b) cumulative event strength correlated with the number of events per day.

Blockage events per day per tuyere	HO1	HO4
2019	64.5	44.9
2020	47.1	62.2
2021	34.2	43.4

Table 1 Number of recorded blockage events per day of and tuyere for BF 1 and BF 4 at voestalpine Donawitz.

Fig.2: Example of a damaged tuyere. (photo courtesy of voestalpine Donawitz).

Stefan Puttinger | stefan.puttinger@jku.at

SELECTED PUBLICATION

Atzori M., Vinuesa R., Schlatter P. Control effects on coherent structures in a non-uniform adverse-pressure-gradient boundary layer, in: International Journal of Heat and Fluid Flow, Volume 97, 2022.

Balachandran Nair A., Pirker S., Saeedipour M. Resolved CFD-DEM simulation of blood flow with a reduced-order RBC model, in: Computational Particle Mechanics, Volume 9, Page(s) 759–774, 2022.

Dabbagh F., Schneiderbauer S. Anisotropy characterization of turbulent fluidization, in: Physical Review Fluids, Volume 7, Number 9, Page(s) 094301, 2022.

Puttinger S., Saeedipour M. Time-resolved PIV measurements of a deflected submerged jet interacting with liquid- gas and liquid-liquid interfaces, in: Experimental and Computational Multiphase Flow, Volume 4, Number 2, Page(s) 175-189, 2022.

Rauchenzauner S., Schneiderbauer S. Validation study of a Spatially-Averaged Two-Fluid Model for heat transport in gas-particle flows, in: International Journal of Heat and Mass Transfer, Volume 198, Page(s) 123382, 2022.

Saeedipour M., Pirker S. Analysis of Hysteresis in the Regime Transition of Cocurrent Liquid-Gas Flow, in: Steel Research International, 2022.

Saeedipour M., Schneiderbauer S. Toward a universal description of multiphase turbulence phenomena based on the v orticity transport equation, in: Physics of Fluids, Volume 34, Number 7, Page(s) 073317, 2022.

Schneiderbauer S., Saeedipour M. The impact of interphase forces on the modulation of turbulence in multiphase flows, in: Acta Mechanica Sinica, Volume 38, Page(s) 721446, 2022.